Application of a Lumped-Inertia Technique to Vibrational Analysis of the Torsional-Twisting Modes of Low Molecular Weight Polyphenylenes and Polyethynylphenylenes

Xiange Zheng, Natalie Vedova-Brook, and Karl Sohlberg*

Department of Chemistry, Drexel University, 3141 Chestnut Street, Philadelphia, Pennsylvania 19104

Received: September 5, 2003; In Final Form: December 19, 2003

The vibrational dynamics of nanosystem components are likely to play a critical role in both nanomechanical and nanoelectronic systems. We demonstrate that vibrational analysis with a lumped-inertia technique can efficiently and reliably anticipate certain vibrational properties without the need for performing costly comprehensive full normal-mode computations. Three classes of linear oligomers with potential for application in nanoelectronics are investigated with this technique. The torsional-twisting frequencies from the lumped-inertia model accurately reproduce the frequencies computed with full normal-mode analysis based on electronic structure calculations. The lumped-inertia model reveals the importance of long-range coupling in torsional-twisting dynamics and affords a partitioning of the effect of phenyl ring substituents on the torsional vibrational frequencies between inertial and electronic structure contributions.

Introduction

One proposed molecular electronic switching scheme is to capitalize on changes in conductivity that accompany changes in the relative alignment of phenyl rings along a polyphenyl chain. Theoretical work has predicted that the conductivity of such a conjugated chain may be varied by 10^4 simply by varying the torsional alignment of two adjacent phenyl rings.[1] More recent studies have explored the influence of molecular vibrations in general on molecular conductance.[2] For the *p*-benzenedithiol molecule, it was reported that none of the normal-mode vibrations lead to appreciable changes in conductance, owing to the rigidity of the molecule. By contrast, Di Ventra et al.[3] noted that when the molecule is modified with a NO_2 substituent (2-nitro-1,4-benzene-dithiol), twisting of the NO_2 substituent can lead to appreciable changes in the molecular orbital energies and potentially observable changes in the I/V characteristics. A stunning example of the influence of vibrational motion on molecular electron transport has been demonstrated in C_{60} on a gold surface.[4] The differential conductance through the C_{60} to the gold substrate exhibits features with an energy spacing characteristic of the frequency of the oscillation of the C_{60} relative to the gold surface, about 1.2 THz.

From the above, it is clear that successful nanomachine engineering will depend on the ability to reliably anticipate nanostructure vibrational properties. For nanoelectronics, low-frequency torsional-twisting modes are of particular relevance.[1] The issue of determining low-frequency torsional vibrations also arises during the parametrization of molecular mechanics force fields[5−7] and are important for developing reliable potential functions for use in condensed-phase simulations.[8] Previously it has been demonstrated that continuum methods of vibrational analysis, common in mechanical engineering, may be used effectively in the description of bending and flexing vibrations of nanorods and nanotubes.[9] In the same spirit, here we borrow the lumped-inertia technique from mechanical engineering. Recent engineering applications include: Bapat and Bhutani[10] have reported a matrix method for solution to the problem of torsional vibrations of a multistepped shaft with elastically attached masses. Li et al.[11] proposed the initial parameter method and the transfer matrix method for use with concentrated masses coupled by translational springs. A closed form solution was presented by Qiao et al.[12] for torsional vibration of nonuniform shafts with arbitrary distribution of rigid disks. We demonstrate that a similar lumped-inertia technique[12] is efficient and accurate for predicting the frequencies of the low frequency torsional-twisting modes of polyphenylenes and polyethynylphenylenes, species potentially important for nanoelectronics.

Theoretical Methods

To derive force constants and provide benchmark frequencies against which to test the lumped-inertia model, we used two standard electronic structure techniques: HFSCF[13] with the 3-21G* basis set[14,15] and AM1.[16] Admittedly, these methods are very approximate, but they are in common use for molecular systems and the typical scaling factors are well known.[17] The computations in this study are based mainly on HFSCF. AM1 calculations were used to demonstrate the extension of lumped-inertia methods to larger systems. Supporting the choice of HFSCF is the finding by Scott and Radom[17] that HF methods yield low frequencies that are of comparable reliability to those produced by density functional theory (DFT) calculations. We carried out test calculations and found similar agreement. (See subsection 5 of Results and Discussion.) The techniques chosen here are, of necessity, sufficiently efficient for full normal-coordinate analysis of oligomers with several primitive units. This provides a reasonable set of frequency data from which to derive torsional force constants. Except where specifically noted to the contrary, all structures were fully optimized and display

* Author to whom correspondence may be addressed. E-mail: sohlbergk@drexel.edu.

10.1021/jp036659j CCC: $27.50
Published on Web 03/05/2004

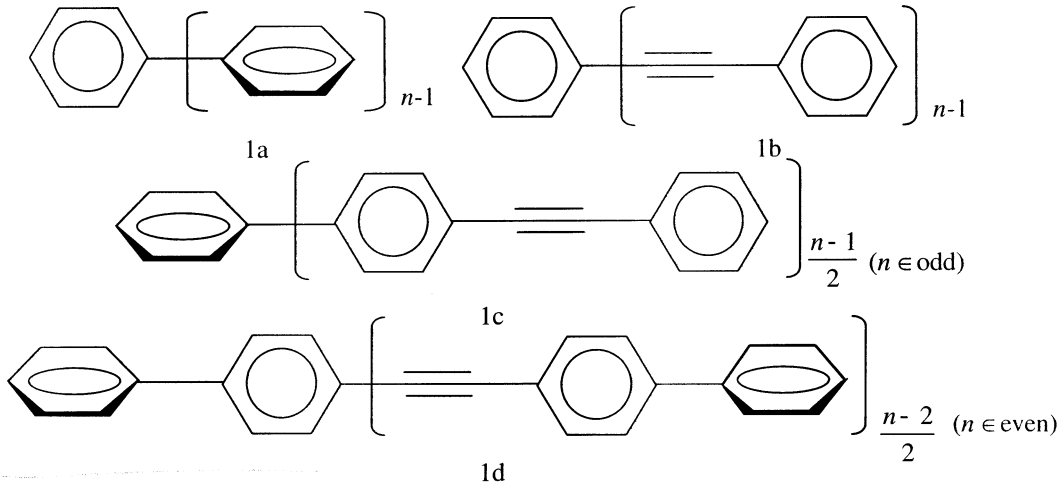

Figure 1. Schematic drawings of the three classes of molecules considered in this study. When optimized at the HFSCF level, the structures are as follows: For the single-bond molecules (a), the dihedral angles are 49−50° and −49 to −50°, alternatively, for every other pair of two adjacent phenyl rings, which renders alternate benzene rings parallel to each other. For triple-bond molecules (b), the dihedral angles are 0°, which makes all phenyl rings parallel to one another. For the molecules with a mixture of both single and triple bonds (c and d with odd and even values of n respectively), the dihedral angles are 0° between two adjacent phenyl rings connected with a triple-bond linkage. The dihedral angles are 49−50° for all other pairs of adjacent phenyl rings bonded with a single bond.

only positive real eigenvalues of the Hessian matrix. The convergence criterion for structural optimization was set to be atypically stringent (≤0.00001 Hartree/Bohr) for more accurate treatment of the low-frequency vibrational modes upon subsequent frequency analysis. Torsional modes were identified by visualization.

We have chosen to study torsional modes in three classes of molecules, shown in Figure 1: (i) single-bond species (Figure 1a), studied by Samanta et al. for molecular wire applications;[1] (ii) triple-bond species (Figure 1b), studied by Chen et al. for molecule electronic device applications;[18] and (iii) mixed species with alternating single- and triple-bond linkages between adjacent phenyl rings (parts c and d of Figure 1).

We note that, if one is principally interested in torsional-twisting modes of these linear oligomers, considerable simplification of the vibrational analysis can be achieved through application of the lumped-inertia technique. The vibrational features for the torsional-twisting modes of the molecule are described as relative rotations of "lumped inertias" about the principal axis of the molecule. Each component ring is modeled as a rigid body with inertia equal to that of the ring and its attached hydrogens (and any substituents present). Adjacent inertias are taken to interact with force constants to be derived in the discussion section. This procedure effectively drops the higher-frequency modes from the vibrational analysis,[19] thereby reducing the vibrational analysis from one of $3N - 6$ normal modes (N is the number of atoms in the molecule) to $n - 1$ torsional modes (n is the number of rings in the polyphenyl chain). For an n-ring oligomer, this results in an approximately 30-fold decrease in the number of degrees of freedom. Since vibrational analysis involves matrix diagonalization, which scales with the cube of the number of degrees of freedom, this simplification can result in a very significant decrease in the computational expense for large systems and should make accessible even larger systems, for which full normal-mode calculations are intractable.

For an n-ring linear oligomer (single- or triple-bond species) as presented in Figure 1 (parts a and b), when all long-range coupling is considered, the equations of torsional motion (corresponding to the twist modes) may be given in terms of the angular positions of each lumped inertia as follows

$$I^j\ddot{\theta}_1 = k_1(\theta_2 - \theta_1) + k_2(\theta_3 - \theta_1) + k_3(\theta_4 - \theta_1) + \cdots + k_j(\theta_{j+1} - \theta_1) + \cdots + k_{n-1}(\theta_n - \theta_1) = -(\sum_{l=1}^{(n-1)} k_l)\theta_1 + \sum_{l=1}^{(n-1)} (k_l\theta_{l+1}) \quad (j = 1) \quad (1)$$

$$I^j\ddot{\theta}_j = -k_1(\theta_j - \theta_{j-1}) - k_2(\theta_j - \theta_{j-2}) - k_3(\theta_j - \theta_{j-3}) - \cdots - k_{j-1}(\theta_j - \theta_1) + k_1(\theta_{j+1} - \theta_j) + k_2(\theta_{j+2} - \theta_j) + k_3(\theta_{j+3} - \theta_j) + \cdots k_{n-j}(\theta_n - \theta_j) = \sum_{l=1}^{(j-1)} (k_l\theta_{j-l}) - (\sum_{l=1}^{(j-1)} k_l + \sum_{m=1}^{(n-j)} k_m)\theta_j + \sum_{l=1}^{(n-j)} (k_l\theta_{j+l}) \quad (1 < j < n) \quad (2)$$

and

$$I^j\ddot{\theta}_j = -k_1(\theta_n - \theta_{n-1}) - k_2(\theta_n - \theta_{n-2}) - k_3(\theta_n - \theta_{n-3}) - \cdots - k_{n-1}(\theta_n - \theta_1) = \sum_{l=1}^{(n-1)} (k_l\theta_{n-l}) - (\sum_{l=1}^{n-1} k_l)\theta_n \quad (j = n) \quad (3)$$

Symbolically

$$\ddot{\vec{\theta}} = \mathbf{M}\vec{\theta} \quad (4)$$

where θ_j is the angular position of the jth phenyl ring relative to its position at equilibrium and I^j is the moment of inertia of the jth phenyl ring about the twist axis, which is I^j_{zz} corresponding to the moment about the primary axis (z axis) in our case (I^j_{zz} = 87 amu Å^2 $\forall$ j). k_l (l = 1, 2, ..., $n - 1$) is the torsional force constant between the target ring and its lth-nearest neighbor. $\mathbf{M}$ is an $n \times n$ matrix where n is the number of rings in the molecule under consideration, which is eq 5, shown in

CHART 1

$$\mathbf{M} = \frac{1}{I}\begin{bmatrix} -\sum_{l=1}^{(n-1)} k_l & k_1 & k_2 & k_3 & \cdots & k_{j-1} & \cdots & k_{n-1} \\ k_1 & -(k_1 + \sum_{l=1}^{(n-2)} k_l) & k_1 & k_2 & \cdots & k_{j-2} & \cdots & k_{n-2} \\ k_2 & k_1 & -(k_1 + k_2 + \sum_{l=1}^{(n-3)} k_l) & k_1 & \cdots & k_{j-3} & \cdots & k_{n-3} \\ k_3 & k_2 & k_1 & -(k_1 + k_2 + k_3 + \sum_{l=1}^{(n-4)} k_l) & & & \cdots & k_{n-4} \\ \vdots & & \vdots & & \vdots & & & \vdots \\ k_{j-1} & k_{j-2} & \cdots & k_1 & -(\sum_{l=1}^{(j-1)} k_l + \sum_{l=1}^{(n-j)} k_l) & & \cdots & k_{n-j} \\ \vdots & & \vdots & & \vdots & & & \vdots \\ k_{n-1} & k_{n-2} & \cdots & \cdots & k_{n-j} & \cdots & k_1 & -\sum_{l=1}^{(n-1)} k_l \end{bmatrix} \quad (5)$$

Chart 1 where $I = I_{zz}$. In the standard way, we write the solution to eq 4 in the form

$$\vec{\theta} = \vec{C}\, e^{-i\nu t} \quad (6)$$

where $\vec{C}$ is a vector of coefficients, $i = (-1)^{1/2}$, t is time, and ν is a vibrational frequency.[20] It follows that

$$\mathbf{M}\vec{C} = -\nu^2\vec{C} \quad (7)$$

By solving the eigenvalue problem (eq 7), we obtain the eigenvalues ν^2 in terms of force constants k_1, k_2, ..., k_{n-1} and the moment of inertia I_{zz}, each of which is a multivariable expression. Specifically, when all k_l except for k_1 were assumed to be zero ($k_l = 0$ for $l = 2$, ..., $n - 1$), that is, when all long-range coupling is ignored (only nearest-neighbor interactions are considered), the above matrix simplifies into a tridiagonal form, and the eigenvalues are of the form

$$\nu_{\text{theo}}^{n,i}(k,I_{xx}) = W_{\text{theo}}^{n,i}(k/I_{zz}^{n,i})^{1/2} \quad (8)$$

where $W_{\text{theo}}^{n,i}$ is the coefficient corresponding to each eigenvalue $\nu_{\text{theo}}^{n,i}(k,I_{zz})$. The units of $\nu_{\text{theo}}^{n,i}(k,I_{zz})$ and I_{zz} are in s^{-1} and amu Å^2, respectively. These eigenvalues contain the frequencies corresponding to the twist modes and are presented in Table 1 denoted ν_{theo}.

Clearly, based on the above matrix (5), the use of a nearest-neighbor linear response theory results in a tridiagonal form, where all elements except those along the diagonal and its neighboring element(s) are zero. Second- and third-nearest-neighbor interactions may be taken into account in a straightforward manner. The most significant complication is that the coupling matrix changes from tridiagonal form to penta- and heptadiagonal form, respectively. Computations at all three levels of coupling are reported below.

Results and Discussion

Table 2 shows calculated torsional vibration frequencies (ω_{HF} and ω_{AM1}) for n-ring single-bond molecules based on AM1 and HFSCF calculations. Table 3 shows calculated frequencies for n-ring triple-bond molecules based on HFSCF calculations.

1. Tridiagonal Analysis. To obtain the force constant(s) for each of the lumped molecules, the most straightforward tridiagonal form was first used, which incorporates only the nearest-neighbor interactions. As shown in Table 1, the predicted frequencies are functions dependent only on a single force constant k, which is denoted k_s for single-bond and k_t for triple-bond systems, respectively. We determined the torsional force constants by minimizing the function $\epsilon(k)$, the sum-of-squares of the errors in the predicted frequency (ω_{theo}) as a function of force constant (k_s for 1a and k_t for 1b)

$$\epsilon(k) = \sum_{n=2}^{6}\sum_{i=1}^{n-1}[\omega_{\text{HF}}^{n,i} - \omega_{\text{theo}}^{n,i}(k,I_{zz})]^2 \quad (9)$$

For single-bond species, based on HFSCF calculations, the derived force constant k_s was 13.8 kcal/mol from the entire data set, while k_s = 14.1, 13.8, 13.9, 13.6, and 13.7 kcal/mol using only the n = 2, 3, 4, 5, and 6 systems, respectively. Substituting the derived global force constant (k_s = 13.8) into the theoretical expressions for the frequencies for each single-bond species (n = 2−6) presented in Table 1, the theoretical values of the frequencies for these molecules were obtained (predicted) and compared to those from the electronic structure calculations.

For the triple-bond species, the force constant (k_t) for triple-bond torsions was derived in the same manner as for the single-bond torsions and found to have the value k_t = 1.08 kcal/mol based on the HFSCF calculations from the entire data set. (This corresponds to the minimal value of the error function of frequency ω as a function of force constant (k_t) as shown in expression 9). The k_t values derived from each individual system with n = 2−6 are in the range of 0.95−1.11 kcal/mol, which is in excellent agreement with k_t derived from the entire data set, similar to the situation for single-bond torsions. Note that, unsurprisingly, the coupling of two rings connected by the C−C≡C−C bond linkage is ∼10 times weaker than the coupling through a single bond only. Theoretical frequencies are obtained by substituting the theoretical force constant derived above into the corresponding expressions of frequencies shown in Table 1. Figure 2 shows the calculated (at HFSCF level, ω1−ω5 series) and predicted frequencies using the tridiagonal matrix (ω1′−ω5′ series) and pentadiagonal matrix (ω1″−ω5″ series) for the single-bond linear oligomers (n = 2−6).

Note in Figure 2 that there are important discrepancies between the theoretical frequencies from the tridiagonal fitting and those from the HFSCF calculations for the lowest-frequency modes. These discrepancies increase in both absolute and relative importance with increasing n. To investigate this

TABLE 1: Theoretical (ν_{theo}) Frequencies of Pure Single- and Triple-Bond Species Based on Tridiagonal Fitting

n[a]	ν_{theo} (s^{-1})	n[a]	ν_{theo} (s^{-1})
2	$\left(\frac{2}{I_{zz}}\right)^{1/2}(k)^{1/2} = 1.414\left(\frac{k}{I_{zz}}\right)^{1/2}$	5	$\left(\frac{3-(5)^{1/2}}{2I_{zz}}\right)^{1/2}(k)^{1/2} = 0.618\left(\frac{k}{I_{zz}}\right)^{1/2}$
3	$\left(\frac{1}{I_{zz}}\right)^{1/2}(k)^{1/2} = \left(\frac{k_s}{I_{zz}}\right)^{1/2}$		$\left(\frac{5-(5)^{1/2}}{2I_{zz}}\right)^{1/2}(k)^{1/2} = 1.176\left(\frac{k}{I_{zz}}\right)^{1/2}$
	$\left(\frac{3}{I_{zz}}\right)^{1/2}(k)^{1/2} = 1.732\left(\frac{k}{I_{zz}}\right)^{1/2}$		$\left(\frac{3+(5)^{1/2}}{2I_{zz}}\right)^{1/2}(k)^{1/2} = 1.618\left(\frac{k}{I_{zz}}\right)^{1/2}$
4	$\left(\frac{2-(2)^{1/2}}{I_{zz}}\right)^{1/2}(k)^{1/2} = 0.765\left(\frac{k}{I_{zz}}\right)^{1/2}$		$\left(\frac{5+(5)^{1/2}}{2I_{zz}}\right)^{1/2}(k)^{1/2} = 1.902\left(\frac{k}{I_{zz}}\right)^{1/2}$
	$\left(\frac{2}{I_{zz}}\right)^{1/2}(k)^{1/2} = 1.414\left(\frac{k}{I_{zz}}\right)^{1/2}$	6	$\left(\frac{2-(3)^{1/2}}{I_{zz}}\right)^{1/2}(k)^{1/2} = 0.518\left(\frac{k}{I_{zz}}\right)^{1/2}$
	$\left(\frac{2+(2)^{1/2}}{I_{zz}}\right)^{1/2}(k)^{1/2} = 1.848\left(\frac{k}{I_{zz}}\right)^{1/2}$		$\left(\frac{1}{I_{zz}}\right)^{1/2}(k)^{1/2} = 1.000\left(\frac{k}{I_{zz}}\right)^{1/2}$
			$\left(\frac{2}{I_{zz}}\right)^{1/2}(k)^{1/2} = 1.414\left(\frac{k}{I_{zz}}\right)^{1/2}$
			$\left(\frac{3}{I_{zz}}\right)^{1/2}(k)^{1/2} = 1.732\left(\frac{k}{I_{zz}}\right)^{1/2}$
			$\left(\frac{2+(3)^{1/2}}{I_{zz}}\right)^{1/2}(k)^{1/2} = 1.932\left(\frac{k}{I_{zz}}\right)^{1/2}$

[a] Number n is the number of phenyl rings contained in the molecule under consideration. $\nu_{theo} = \omega_{theo}c$ (c is the speed of light).

TABLE 2: Calculated Frequencies in cm^{-1} of Single-Bond Oligomers at the HFSCF and AM1 Levels

n[a]	ω_{HF} (cm^{-1})	ω_{AM1} (cm^{-1})
2	61.6	71.0
3	42.7	59.2
	74.8	83.2
4	35.5	50.9
	61.9	71.1
	80.3	86.8
5	28.4	47.3
	50.6	62.9
	70.3	78.5
	82.7	88.5
6	26.2	45.3
	45.0	57.5
	62.1	71.1
	75.7	82.6
	83.2	86.6
7	N/A[b]	43.9
		53.7
		65.3
		76.5
		85.2
		87.1
8	N/A[b]	43.1
		50.9
		60.9
		71.1
		80.1
		86.9
		101.5

[a] Number n is the number of phenyl rings contained in the molecule under consideration. [b] Number not available due to computational expense.

TABLE 3: Calculated Frequencies of Triple-Bond Molecules at the HFSCF Level

n	ω_{HF} (cm^{-1})
2	16.0
3	13.2
	19.4
4	11.0
	17.6
	23.0
5	9.3
	14.5
	19.4
	23.0
6	5.3
	11.5
	16.1
	20.0
	23.1

phenomenon, we explored whether any of the following possible physical origins give rise to the discrepancy: (i) n-dependent force constants, (k^n), i.e., force constants that depend on the length of the molecule; (ii) position-dependent k, i.e., force constants that depend on the position of the corresponding bond within the molecule; (iii) mixing of torsional and breathing modes; and (iv) long-range coupling, i.e., coupling of non-adjacent rings.

Theoretical and computational analyses reveal that i, ii, and iii give little or no correction to above discrepancy as we now summarize briefly.

In case i, we derived a unique k^n for each individual system of length n. These differed little from the global k, and their use in the theoretical expressions did not yield frequencies in significantly improved agreement with those from the HFSCF calculations. This result is confirmed by our more elaborate models below.

In case ii, we derived unique k values for each symmetry-unique bond in the molecule. For example, in the $n = 4$ single-

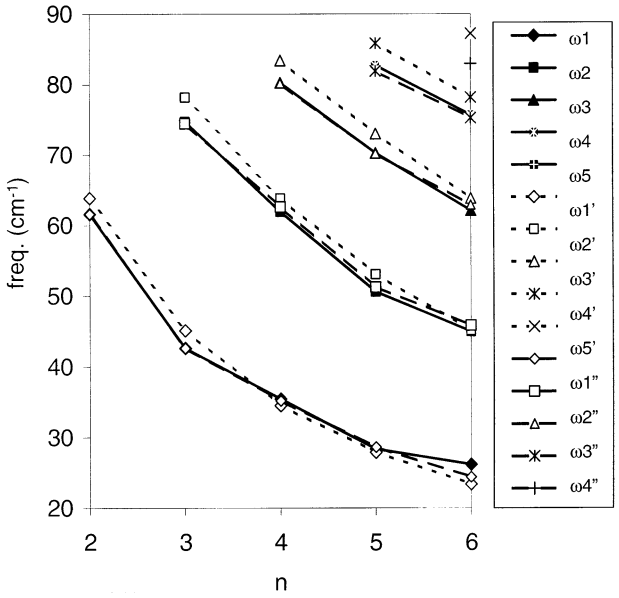

Figure 2. Calculated frequencies for single-bond linear oligomers ($n = 2-6$) in cm^{-1} from HFSCF computation ($\omega1-\omega5$ series, solid lines) and theoretical values from the tri- ($\omega1'-\omega5'$ series, dotted lines) and penta- ($\omega1''-\omega5''$ series, dashed lines) fittings. The heptadiagonal data are not shown but would be visually indistinguishable from the HFSCF data. Line segments connect points of different n that are computed with the same theoretical model.

bond system, the force constant coupling the 1st and 2nd rings was taken to equal that coupling the 3rd and 4th rings, but the force constant coupling the 2nd and 3rd rings was allowed to be unique. Upon fitting to the HFSCF data, however, the two force constants optimized to nearly identical values and led to no improvement in the agreement between the theoretical and HFSCF frequencies.

In case iii, we observed, by visualization, some degree of ring "breathing" whereby the phenyl rings expand slightly near the maximum displacements along the twisting mode and contract to their normal size in the vicinity of the equilibrium. (In the case of biphenyl, the equilibrium corresponds to an angle of about 49° between the planes of the two rings. See also Figure 1.) The C−H bond length as a function of the displacement of the torsional angle from equilibrium shows harmonic dependence. A displacement of 10 degrees from equilibrium stretches the C−H (C−C) bonds by 0.223 (0.282)% and displacement of the torsional angle by 20° results in a stretch of 0.949 (1.146)%. One might speculate that such ring breathing could change the effective inertia of the ring, thereby altering the vibrational frequencies. Consider a one-dimensional model of the effect of this ring breathing and its Taylor series approximation. The differential equation of motion may be given as

$$\ddot{\theta} = -k\theta/(I + \alpha\theta^2) \approx -k\theta/I + 6\alpha k\theta^3/I^2 \qquad (10)$$

where α is a small empirical parameter that effectively increases the magnitude of the denominator for large displacements of the angular coordinate θ from equilibrium, mimicking an increase in the inertia I. From this expression, it is clear that mixing of the ring-breathing mode cannot account for the observed *increase* in the low frequencies over that predicted with the linear model. First of all, since α does not appear in the leading term of the expansion, it will have no effect on the frequency of small oscillations. Even if finite displacements are considered, the second term will have the effect of weakening

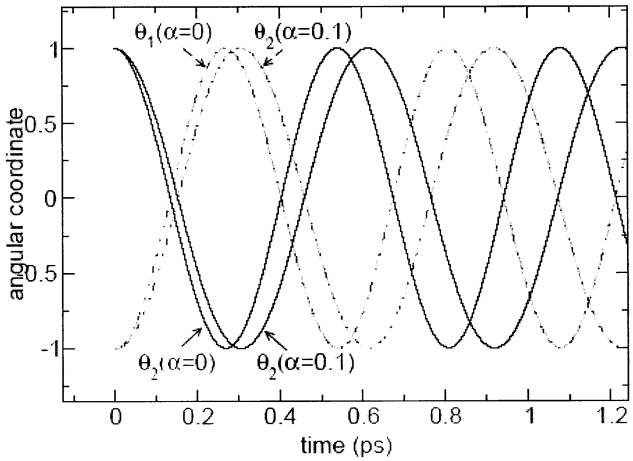

Figure 3. Time dependence of the angular coordinate variables θ_1 and θ_2 over a few periods of oscillation of biphenyl. α is an empirical parameter that sets the strength of the coupling between the torsional and breathing vibrations of the phenyl rings. For $\alpha = 0.0$, the period is 0.54 ps, corresponding to $\omega = 61$ cm^{-1}, and for $\alpha = 0.1$, the period is 0.61 ps, corresponding $\omega = 54$ cm^{-1}. Note that coupling to ring breathing has the effect of decreasing the frequency of torsional oscillation.

the effective restoring force, which would decrease the associated frequency. This is opposite to the observed result.

To further illustrate the effect of coupling the breathing mode to the torsional vibrations, a numerical integration was undertaken to solve the corresponding nonlinear differential equations for biphenyl (the single-bond $n = 2$ species)

$$d^2\theta_1/dt^2 = -k_s(\theta_2 - \theta_1)/[I + \alpha(\theta_2 - \theta_1)^2] \qquad (11a)$$

$$d^2\theta_2/dt^2 = k_s(\theta_2 - \theta_1)/[I + \alpha(\theta_2 - \theta_1)^2] \qquad (11b)$$

where θ_1 and θ_2 are the angular coordinate variables of the two rings on biphenyl. Figure 3 shows the time dependence of θ_1 and θ_2 over a few periods of oscillation of biphenyl for the cases of $\alpha = 0.0$ (period 0.54 ps corresponds to $\omega = 61$ cm^{-1}) and $\alpha = 0.1$ (period 0.61 ps corresponds to $\omega = 54$ cm^{-1}). The time period when α is nonzero is larger, and therefore the frequency is smaller. Thus, the coupling of the ring breathing, reflected by a nonzero value of parameter α, produces a decrease in the torsional vibration frequency. This is exactly what is predicted with a simple analytical model. Therefore, coupling to the breathing mode does not explain the observed deviation of the low frequencies from what is predicted by a nearest-neighbor coupling model.

In case iv, we found that inclusion of long-range coupling completely resolves the issue, as we now present in detail.

2. Pentadiagonal Fitting. With the second-nearest-neighbor coupling taken into account, the matrix presented in eq 5 becomes pentadiagonal in form. By solving the corresponding eigenvalue problem, the theoretical frequencies for each system are functions in terms of two force constants, the primary one k_1 and the secondary one k_2, which account for the nearest- and second-nearest-neighbor interactions, respectively. By minimization the same sum-of-squares of the errors function presented in eq 9, the force constants were derived for each system. Table 4 presents the force constants derived from the pentadiagonal fitting of the HFSCF results for single bond species. The secondary force constant (k_{s2}), which is an indication of the strength of the long-range coupling, is 10 times lower than that of the primary one (k_{s1}). As n increases, k_{s2} becomes larger and

TABLE 4: Predicted Force Constants Based on the Pentadiagonal (Heptadiagonal for $n = 6$ Species) Fitting of HFSCF Results for Single-Bond Species

n	k_{s1}	k_{s2}
2	14.1	N/A[a]
3	13.2	−0.1
4	13.9	0.6
5	13.6	0.6
6	13.7 (13.7)	0.8 (0.3, ($k_{s3} = 0.6$))

[a] For the $n = 2$ species, there is no second-nearest neighbor therefore no secondary force constant k_{s2}. [b] k_{s3} is the tertiary force constant from the heptadiagonal fitting.

TABLE 5: Predicted Force Constants Based on Pentadiagonal Fitting of HFSCF Results for Triple-Bond Species

n	k_{t1}	k_{t2}
2	1.0	N/A[a]
3	1.0	0.2
4	1.1	0.1
5	1.0	0.2
6	1.1	0.0

[a] For the $n = 2$ species, there is no second-nearest neighbor therefore no secondary force constant (k_{t2}).

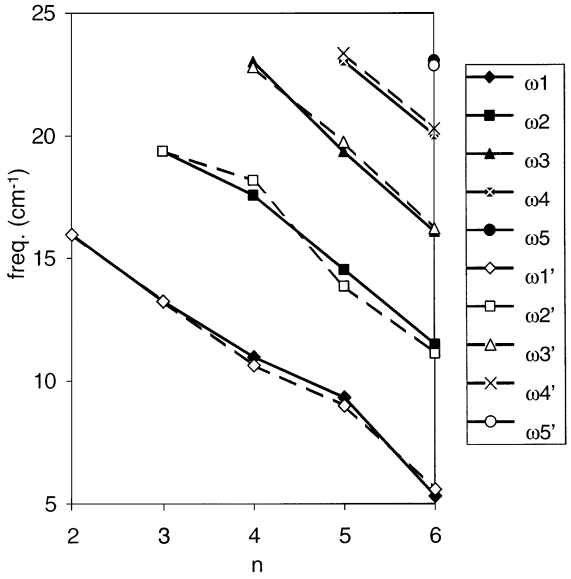

Figure 4. Frequencies calculated at the HFSCF level ($\omega1-\omega5$ series, solid lines) and predicted ($\omega1'-\omega5'$ series, dashed lines) using the pentadiagonal matrix for triple bond linear oligomers ($n = 2-6$) in cm^{-1}.

therefore the contribution from the long-range coupling becomes more important. This result is consistent with the expected more significant conjugation in longer systems (in hindsight, a chemically intuitive result).

The calculated (at HFSCF level, $\omega1-\omega5$ series) and predicted ($\omega1''-\omega5''$ series) frequencies for the single-bond linear oligomers ($n = 2-6$) based on pentadiagonal fitting are shown in Figure 2. The predicted frequencies are in excellent agreement with the ones from HFSCF calculations, indicating that the lumped-inertia treatment accurately recovers the torsional-twisting frequencies for the singe-bond species.

For the triple-bond molecules, the primary and secondary force constants k_{t1} and k_{t2} were found using the same procedure. The derived force constants for $n = 2-6$ systems are provided in Table 5.

By substituting the force constants acquired here into the expressions for the theoretical frequencies derived from the pentadiagonal fitting, the predicted frequencies were obtained for each species and are presented in Figure 4 together with the calculated frequencies. Again, similar to the situation for the single-bond systems, the predicted frequencies agree well with the calculated ones at the HFSCF level. The lumped-inertia pentadiagonal fitting successfully recovers the torsional-twisting frequencies for the triple bond systems. Note that in both the single-bonded and triple-bonded species, k_1 is almost invariant with n, consistent with our earlier conclusion that a length-dependent force constant is not at the root of the unexpectedly high, low-frequency vibrations.

3. Heptadiagonal Fitting. It may be seen in Figure 2 that, for the $n = 6$ system, there is some residual discrepancy between the theoretical frequency using the pentadiagonal matrix and HFSCF frequency for the lowest-frequency torsional-twisting mode. Given the observed importance of long-range coupling, we carried out calculations including second- and third-nearest-neighbor coupling. This results in a heptadiagonal matrix form involving primary (k_1), secondary (k_2), and tertiary (k_3) force constants. The best-fit force constants for the $n = 6$ single-bond system are given parenthetically in Table 4. The derived theoretical frequencies are visually indistinguishable from the HFSCF data when superimposed upon Figure 2, which indicates that the inclusion of this extra-long-range coupling yields excellent agreement between the theoretical and HFSCF results. Obviously, by including sufficiently many fitting parameters, the theoretical model can recover the computed vibrational frequencies, but the results presented herein show clearly that long-range coupling is at play in the torsional-twisting dynamics of polyphenylenes.

TABLE 6: Predicted Force Constants Based on the Pentadiagonal Fitting of AM1 Results for Single-Bond Species

N	k_{s1}	k_{s2}
2	18.8	N/A[a]
3	17.2	4.5
4	15.4	5.2
5	14.6	5.3
6	13.1	6.4
7	12.9	6.4
8	14.8	5.9

[a] For the $n = 2$ species, there is no second-nearest neighbor therefore no secondary force constant.

To demonstrate how the lumped-inertia technique might be applied to larger oligomers ($n > 6$), we repeated the procedure using full normal-coordinate analysis on oligomers $n = 1, 2, ..., 8$ of the single-bond species at the semiempirical AM1[16] level of theory, which is sufficiently efficient for practical calculations on larger systems. Table 6 shows the predicted force constants based on pentadiagonal fitting using the AM1 results. It reveals the same phenomenon as when HFSCF data is used, that the contribution from long-range coupling becomes generally more important with increasing n. The absolute value of the predicted secondary force constant k_{s2} based on AM1 computation is predicted to be about 10 times higher than that from HFSCF computation for the same system, suggesting that AM1 overestimates the long-range coupling. Unfortunately, we were unable to extend the treatment to larger oligomers of the triple-bonded species with AM1 semiempirical calculations as we did in the case of the single bond oligomers. All frequencies for torsional-twisting modes of the triple-bond systems from

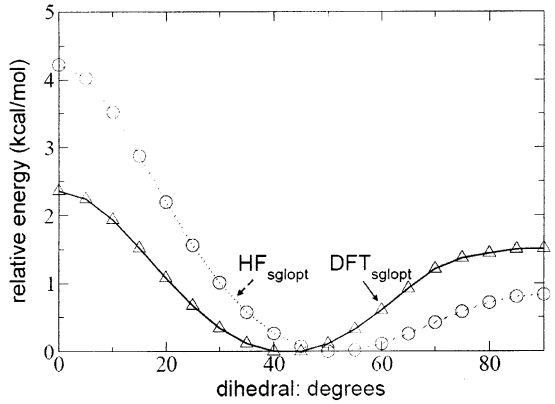

Figure 5. Relative energies from restricted optimizations of biphenyl at both HF and DFT levels, denoted HF_{sglopt} and DFT_{sglopt}, respectively. Energies at each level are referenced to the lowest-energy structure at the same level.

AM1 calculations are almost the same ($\sim$45.0 cm^{-1}) for all values of *n*, which is physically nonsensible.

From AM1 calculations, as shown in Table 2, we note that the lowest computed frequencies appear to be approaching a constant ($\sim$45 cm^{-1}) with increasing *n*, while the predicted frequencies continue to decrease. This could be a shortcoming of the lumped-inertia model; however, it is more likely that the AM1 method fails to accurately capture the lowest-frequency vibrations. The complete failure of the AM1 method for the triple bond species lends credence to the latter possibility. As reported previously,[21−23] the energy barriers to internal rotation are often underestimated by AM1 and may arise from an inadequacy of the AM1 empirical nuclear repulsion functions.

4. Validation. For validation, we first note that the primary force constants derived here are all quite similar for systems of similar chemistry. Furthermore, the force constant of 14.1 kcal/mol, obtained here for $n = 2$ single-bond system, is in good agreement with the value of 14.6 kcal/mol, derived by calculating the second derivative of expression

$$V(\phi) = \sum_{n=1}^{m} \frac{1}{2} V_n(1 - \cos n\phi)$$

where $n = 2$, 4, and 6 and $V_1 = 0.10$, $V_2 = -1.90$, and $V_3 = -0.27$ results from a B3LYP/6-311+G(d,p) calculation provided in ref 24.

As mentioned above, for single-bond polyphenyl molecules, the adjacent rings are offset by $\sim$45° to each other in the optimized structures. As a validation check, constrained optimizations were performed at both the B3LYP and HF levels for biphenyl, with the dihedral angle between the two phenyl rings fixed at 0, 5, 10, ..., 85, and 90° successively (at a 5° interval). As shown in Figure 5, in the lowest-energy configuration, biphenyl adopts a very similar offset structure at the HF and DFT levels, a dihedral angle of 45 and 50°, respectively. Note also that the curvatures of the two potentials at their respective minima are similar. The trends in structural preference captured here are consistent with those reported by Karpfen et al.[24]

5. Mixed Systems with Alternating Single- and Triple-Bond Linkage. For the mixed system with both single- and triple-bond linkages between adjacent rings, the second-nearest neighbor is sufficiently far from the target ring to reduce long-range coupling; therefore, the tridiagonal matrix is an appropriate form for the treatment of the ring coupling in such systems.

TABLE 7: Calculated (ω_{HF}) and Predicted (ω_{pred}) Frequencies of the Mixed System at HFSCF Level[a]

n[b]	ω_{HF} (cm^{-1})	ω_{pred} (cm^{-1})	% error
3	14.5	14.1	2.76
	61.8	61.5	0.49
4	10.9	11.4	4.59
	60.8	60.9	0.16
	61.8	62.0	0.32
5	11.3	9.4	16.80
	15.1	15.6	3.31
	61.6	61.1	0.81
	62.6	62.4	0.32
6	N/A	8.0	N/A
		14.1	
		60.9	
		61.5	
		62.6	

[a] The RMS error is 6%. [b] Number *n* is the number of phenyl rings contained in the molecule under consideration.

The equation for vibration motions shown in eq 4 also applies, and the matrix **M** is

$$\mathbf{M}_{mix-odd} = (1/I)\begin{bmatrix} -k_s & k_s & 0 & \cdots & \cdots & \cdots & \cdots & 0 \\ k_s & -k_s-k_t & k_t & 0 & \cdots & \cdots & \cdots & 0 \\ 0 & k_t & -k_s-k_t & k_s & 0 & \cdots & \cdots & 0 \\ \cdots & \cdots & & & & & \cdots & \cdots \\ 0 & \cdots & 0 & k_s & -k_s-k_t & k_t & 0 & 0 \\ 0 & \cdots & \cdots & 0 & k_t & -k_s-k_t & k_s & 0 \\ 0 & \cdots & \cdots & \cdots & 0 & k_s & -k_s-k_t & k_t \\ 0 & \cdots & \cdots & \cdots & \cdots & 0 & k_t & -k_t \end{bmatrix} \quad (12)$$

when *n* is an odd number for a molecule such as presented in Figure 1c, and it is

$$M_{mix-even} = (1/I)\cdot\begin{bmatrix} -k_s & k_s & 0 & \cdots & \cdots & \cdots & \cdots & 0 \\ k_s & -k_s-k_t & k_t & 0 & \cdots & \cdots & \cdots & 0 \\ 0 & k_t & -k_s-k_t & k_s & 0 & \cdots & \cdots & 0 \\ 0 & 0 & k_s & -k_s-k_t & k_t & 0 & \cdots & 0 \\ \cdots & \cdots & & & & & \cdots & \cdots \\ 0 & \cdots & 0 & k_t & -k_s-k_t & k_s & 0 & 0 \\ 0 & \cdots & \cdots & 0 & k_s & -k_s-k_t & k_t & 0 \\ 0 & \cdots & \cdots & \cdots & 0 & k_t & -k_s-k_t & k_s \\ 0 & \cdots & \cdots & \cdots & \cdots & 0 & k_s & -k_s \end{bmatrix} \quad (13)$$

when *n* is an even number for a molecule such as presented in Figure 1 d. Here k_s and k_t are the averaged theoretical force constants over $n = 2-6$ systems for the single-bond and triple-bond torsions, respectively, derived from the pentadiagonal fitting, which are 13.8 kcal/mol for k_s and 1.03 kcal/mol for k_t, respectively. Substitution of these values of k_s and k_t into the expressions of theoretical frequencies obtained based on matrixes 10 and 11, the frequencies (ω_{pred}) were predicted for the mixed systems. Table 7 shows the results together with the calculated values at the HFSCF level denoted ω_{HF}. The predicted frequencies are in good agreement with those from full normal-mode calculations. The frequencies of molecule with $n = 6$ or more can be easily predicted with the same procedure, but the electronic-structure computations become increasingly demanding and were not performed in our study.

As a further test of the lumped-inertia technique, the same procedures were applied on the triple-bond species ($n = 3$) with

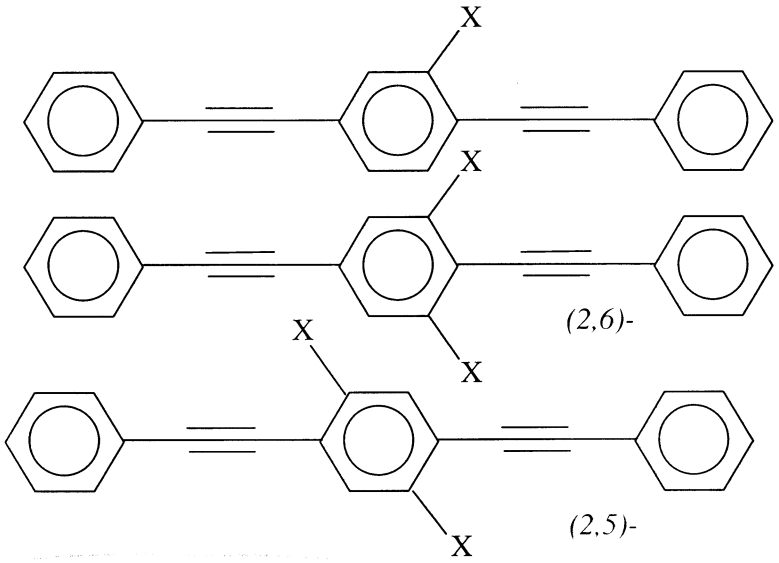

Figure 6. Schematic drawings of the substituted species (X = F, Me). When optimized at the HFSCF level, all phenyl rings are parallel to one another.

TABLE 8: Calculated (ω_{calc}) and Predicted (ω_{pred}) Frequencies of the Substituted System at the HFSCF Level

substituent	ω_{calc} (cm^{-1})	ω_{pred} (cm^{-1})	substituent	ω_{calc} (cm^{-1})	ω_{pred} (cm^{-1})
−H	13.2	11.2	−F ((2,5)-)[b]	17.3	11.7
	19.6	19.4		20.7	14.9
−F[a]	13.8	11.7	−Me ((2,6)-)[b]	14.1	11.7
	18.6	16.4		16.2	14.9
−Me[a]	12.1	11.7	−Me ((2,5)-)[b]	10.9	11.7
	13.6	16.4		14.1	14.9
−F ((2,6)-)[b]	15.0	11.7			
	20.6	14.9			

[a] Species with one substituent −X. [b] Species with two substituents −X.

TABLE 9: Calculated and Predicted Frequencies for Substituted Biphenyl

	−X[a]	σ_m[b]	ω_{HF}[c]	I[d]	k[e]	$\omega_{t1}(k_{ave})$[f]	$\omega_{t2}(k_{biph})$[g]	$\Delta\omega_1$[h]	$\Delta\omega_2$[j]
1	−OH	0.12	48.8	65.5	1.56×10^5	46.6	49.2	2.17	−0.46
2	−NH_2	−0.16	47.9	63.8	1.47×10^5	47.2	49.9	0.70	−1.97
3	−CH_3	−0.07	48.6	63.0	1.49×10^5	47.5	50.2	1.06	−1.62
4	−OCH_3	0.12	44.1	72.6	1.41×10^5	44.3	46.8	−0.18	−2.68
5	−H	0	60.1	44.0	$\mathbf{1.59 \times 10^5}$	56.9	60.1	3.21	0.00
6	−F	0.34	47.8	66.8	1.53×10^5	46.2	48.8	1.64	−0.96
7	−Cl	0.37	42.9	76.5	1.41×10^5	43.1	45.6	−0.19	−2.63
8	−$OCOCH_3$	0.39	42.0	80.9	1.43×10^5	41.9	44.3	0.05	−2.31
9	−$CHCl_2$	0.31	39.4	84.7	1.31×10^5	41.0	43.3	−1.61	−3.93
10	−CHF_2	0.29	41.6	80.2	1.39×10^5	42.1	44.5	−0.55	−2.92
11	−COOH	0.35	41.4	79.4	1.36×10^5	42.3	44.7	−0.95	−3.33
12	−CCl_3	0.4	39.6	85.2	1.33×10^5	40.9	43.2	−1.29	−3.59
13	−$COCH_3$	0.38	43.2	78.8	1.46×10^5	42.5	44.9	0.63	−1.77
14	−CF_3	0.43	40.1	82.4	1.32×10^5	41.6	43.9	−1.49	−3.83
15	−CN	0.56	42.4	75.7	1.36×10^5	43.4	45.8	−0.95	−3.40
16	−NO_2	0.71	41.3	79.3	1.35×10^5	42.4	44.8	−1.09	−3.48
k_{ave} =					1.42×10^5				
k_{biph} =					$\mathbf{1.59 \times 10^5}$				
average difference								0.07	−2.43

[a] Substituent. [b] Substituent parameter.[25] [c] Frequency from HF calculation ω_{HF} in cm^{-1}. [d] Reduced moment of inertia of the entire molecule in amu Å^2. [e] Force constant k based on HF frequency in cm^{-2} amu Å^2. [f] Theoretical frequency ω_{t1} in cm^{-1} using averaged force constant k_{ave}. [g] Theoretical frequency ω_{t2} in cm^{-1} using the force constant of unsubstituted biphenyl molecule k_{biph}. [h] Difference between ω_{HF} and ω_{t1}. [j] Difference between ω_{HF} and ω_{t2}.

one or two substituents on the middle phenyl ring, as shown schematically in Figure 6.

The torsional frequencies for these molecules were predicted by assuming that the introduction of a substituent on the middle phenyl ring does not affect the force constant of the bond between adjacent rings, but changes only the moment of inertia representing the functionalized ring. (This approximation is discussed in detail below.) For an unfunctionalized ring, I_{zz} = 87 amu Å^2. For the monosubstituted system with X = F, I_{zz} = 183 amu Å^2, and I_{zz} = 184 amu Å^2 for X = CH_3. For the dual-substituted system, I_{zz} = 280 amu Å^2 for both X = F and CH_3. In the case of a single substituent, the axis of symmetry is lost so there are no true purely torsional modes. The deviation of the principle moment from the molecular axis is small, however, and the procedure has reasonable predictive power. As shown in Table 8, the agreement of the predicted frequencies with those

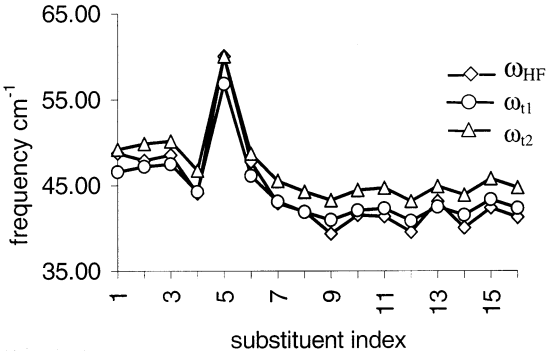

Figure 7. Frequencies from HF calculations ω_{HF}, predicted frequencies ω_{t1} using the averaged force constant k_{ave}, and predicted frequencies ω_{t2} using the force constant for unsubstituted biphenyl k_{biph}.

from HFSCF calculations is quite good. Note that the greatest disagreement is for the F^--substituted species. With the highest electronegativity of all elements, fluorine can be expected to have a larger-than-average effect on the electronic structure of the system, and therefore the assumption that the force constant is independent of substituent is likely less valid.

6. Effect of Substituents on Torsional Frequencies and Force Constants. Calculations were undertaken for dual-substituted, single- and triple-bonded two-ring ($n = 2$) systems to investigate the effect of the presence of substituents on the force constant and torsional frequencies. The 15 substituents considered are listed in Table 9, together with the calculated torsional vibrational frequencies at the HF level ω_{HF}, predicted frequencies ω_{t1} using the average force constant k_{ave}, and predicted frequencies ω_{t2} using the force constant of unsubstituted biphenyl k_{biph}. Note that the predictions are excellent. If the force constant for unsubstituted biphenyl is used, the average difference between theoretical frequencies and the ones from HF calculations, $\omega_{HF} - \omega_{t1}$, is just 2.43 cm^{-1}. If the average force constant is used, the difference $\omega_{HF} - \omega_{t2}$ drops to 0.07 cm^{-1}. Figure 7 shows the three sets of frequencies ω_{HF}, ω_{t1}, and ω_{t2} for the 16 single-bond molecules, with the horizontal axis in the same order shown in Table 9. Obviously, the predicted frequencies track the HF values very well.

The results shown in Table 9 indicate that the relative standard variation in the HF-calculated frequency ω is 11.8%, but the relative standard deviation in force constant k is only 5.9%. Note that the frequency includes contributions from both changes in inertia *and* changes in electronic structure, but force constant k has had the contributions from changes in inertia divided out, so its variation is entirely due to electronic structure effects. Upon the addition of substituents, changes in the torsional frequencies appear to be governed heavily by the changes in the inertias. This result supports the use of k from the unsubstituted species to estimate the frequencies of substituted species by changing only the inertia because k depends weakly on the substituent.

Conclusions

We have applied the lumped-inertia method to torsional-twisting modes of low molecular weight polyphenylene and polyethynylphenylene. The method may be parametrized with very simple systems, for which full ab initio quantum electronic-structure calculations and normal-coordinate analysis are tractable and allows for straightforward prediction of the torsional-twisting frequencies for oligomers of essential arbitrary length. The method is validated by the accurate prediction of the torsional vibrational frequencies for oligomers with mixed single- and triple-bond linkages between adjacent phenyl rings. Excellent accuracy is achieved when coupling through next-nearest-neighbor rings is included (a pentadiagonal matrix form) and demonstrates that the long-range coupling plays an important role in the torsional-twisting dynamics of these systems. Application of the technique to substituted biphenyls allows for a partitioning of the changes in torsional frequencies that take place upon substitution into contributions from changes to the inertial moments and changes to the electronic structure.

Acknowledgment. This work was funded in part by the NSF-NER program, startup funds from Drexel University, and Dupont Corporation in the form of a Dupont Young Professor award to K.S., who also thanks E. T. Sohlberg and J.-M. Yuan for useful discussions and M. Pence for technical assistance.

References and Notes

(1) Samanta, M. P.; Tian, W.; Datta, S.; Henderson, J. I.; Kubiak, C. P. *Phys. Rev. B* **1996**, *53*, R7626−R7629.
(2) Olson, M.; Mao, Y.; Windus, T.; Kemp, M.; Ratner, M.; Leon, N.; Mujica, V. *J. Phys. Chem. B* **1998**, *102*, 941−947.
(3) Di Ventra, M.; Kim, S. G.; Pantelides, S. T.; Lang, N. D. *Phys. Rev. Lett.* **2001**, *86*, 288−291.
(4) Park, H.; Park, J.; Lim, A. K. L.; Anderson, E. H.; Alivisatos, A. P.; McEuen, P. L. *Nature* **2000**, *407*, 57−60.
(5) Allinger, N. L.; Yuh, Y. H.; Lii, J. H. *J. Am. Chem. Soc.* **1989**, *111*, 8551−8565.
(6) Cornell, W. D.; Cieplak, P.; Bayly, C. I.; Gould, I. R.; Merz, K. M.; Ferguson, D. M.; Spellmeyer, D. C.; Fox, T.; Caldwell, J. W.; Kollman, P. A. *J. Am. Chem. Soc.* **1996**, *118*, 2309−2309.
(7) Lii, J. H.; Allinger, N. L. *J. Am. Chem. Soc.* **1989**, *111*, 8566−8575.
(8) Chakrabarti, A.; Yashonath, S.; Rao, C. N. R. *Mol. Phys.* **1995**, *84*, 49−68.
(9) Sohlberg, K.; Sumpter, B. G.; Tuzun, R. E.; Noid, D. W. *Nanotechnology* **1998**, *9*, 30−36.
(10) Bapat, C. N.; Bhutani, N. *J. Sound Vib.* **1994**, *172*, 1−22.
(11) Li, Q. S.; Li, G. Q.; Liu, D. K. *Int. J. Mech. Sci.* **2000**, *42*, 1135−1152.
(12) Qiao, H.; Li, Q. S.; Li, G. Q. *J. Vib. Acoust.* **2002**, *124*, 656−659.
(13) Schmidt, M. W.; Baldridge, K. K.; Boatz, J. A.; Elbert, S. T.; Gordon, M. S.; Jensen, J. H.; Koseki, S.; Matsunaga, N.; Nguyen, K. A.; Su, S. J.; Windus, T. L.; Dupuis, M.; Montgomery, J. A. *J. Comput. Chem.* **1993**, *14*, 1347−1363.
(14) Binkley, J. S.; Pople, J. A.; Hehre, W. J. *J. Am. Chem. Soc.* **1980**, *102*, 939−947.
(15) Pietro, W. J.; Francl, M. M.; Hehre, W. J.; Defrees, D. J.; Pople, J. A.; Binkley, J. S. *J. Am. Chem. Soc.* **1982**, *104*, 5039−5048.
(16) Dewar, M. J. S.; Zoebisch, E. G.; Healy, E. F.; Stewart, J. J. P. *J. Am. Chem. Soc.* **1985**, *107*, 3902.
(17) Scott, A. P.; Radom, L. *J. Phys. Chem.* **1996**, *100*, 16502−16513.
(18) Chen, J.; Reed, M. A.; Rawlett, A. M.; Tour, J. M. *Science* **1999**, *286*, 1550−1552.
(19) Wilson, E. B. J.; Decius, J. C.; Cross, P. C. *Molecular Vibrations*; New York: Dover, 1980 (republished from McGraw-Hill, 1955).
(20) Califano, S. *Vibrational States*; Wiley: London, 1976.
(21) Davila, L. Y. A.; Caldas, M. J. *J. Comput. Chem.* **2002**, *23*, 1135−1142.
(22) Dos Santos, H. F.; Almeida, W. B. *THEOCHEM* **1995**, *335*, 129−139.
(23) Fabian, W. M. F. *J. Comput. Chem.* **1988**, *9*, 369−377.
(24) Karpfen, A.; Choi, C. H.; Kertesz, M. *J. Phys. Chem. A* **1997**, *101*, 7426−7433.
(25) Hansch, C.; Leo, A.; Taft, R. W. *Chem. Rev.* **1991**, *91*, 165−195.